Modelling and Research on a Laminated Tubular Linear Oscillating Generator for Free-piston Stirling Energy Conversion

Rong Guo[1], *Member, IEEE*, Fengyu Zhang[2], Baocheng Guo[3]
[1] School of Electrical and Information Engineering, Beijing University of Civil Engineering and Architecture, Beijing 100044, China
[2] School of the Electrical engineering, University of Nottingham NG7 2RD, U.K
[3] School of Electrical and Automation Engineering, Nanjing Normal University, Nanjing 210046, China

The tubular linear oscillating machine can achieve reciprocating movement directly without auxiliary transmission mechanisms, which is widely used in the Free-piston energy conversion system. To achieve a lower thrust ripple and eliminate the eddy current effect, a circumferential silicon steel stack is usually utilized in the stator, however, it results in assembling difficulties. In this paper, a radially-split lamination tubular linear permanent magnet oscillating machine with auxiliary configuration (RSL-TLPMOMA) is proposed to solve the problem. Firstly, the laminated coefficient expression of split-laminated is deduced, the influence of laminated number and radius ratio on laminated coefficient is discussed, and the optimal combination of the laminated number under different radius ratios is given. Secondly, the subdomain method is used to analyze RSL-TLPMOMA, the auxiliary teeth, slot, and end effect are considered. Finally, a prototype is manufactured and tested.

***Index Terms*— laminated coefficient expression, subdomain conversion method, magnetic field, end effect, auxiliary teeth, tubular linear oscillating machine.**

I. Introduction

The tubular linear permanent magnet oscillation generator (TLPMOG) is a viable option in the Free-piston Stirling energy (FPSE) generating system. It has the advantage of no crank linkage, fast response, simple structure and maintenance-free operation [1] [2].

Many special topologies are developed in the FPSE system[3]-[5]. In[3], a single-phase permanent magnet linear oscillatory generator (LOG) for FPSE is designed and analyzed. The electromagnetic including detent force and eddy-current loss is conducted based on the FEA. In [5], a new radial lamination method is proposed to use in a linear oscillating actuator. The teeth and yoke of the outer stator are laminated in a separated formation. The results indicate that the stacking factor is improved, and this laminated way has a higher back electromotive force (EMF) and thrust.

Due to the particularity of the space environment, the vibration caused by the detent force should be reduced as it will be leading to thrust ripples and a sensitive impact on the system accuracy. To reduce the detent force, auxiliary teeth are introduced in [6]. Since the force prediction is closely related to the magnetic field, therefore, accurate prediction of the magnetic field is essential. At present, several methods are adopted to analyze the magnetic field such as the FEA [7], magnetic equivalent circuit (MEC) method [8], Schwarz-Christoffel (SC) conformal mapping method [9] and subdomain (SD) method [10]. Among these methods, the FEA method can be considered the whole model without simplification, but it is time-consuming. MEC method can take into account the magnetic saturation and armature reaction, however, the force calculation needs to be improved. SC method is an effective consideration of slot effects, but it still has the crowding effect in transformation. So, the SD method is an elegant way of predicting magnetic fields.

Corresponding author: Rong Guo (e-mail:18813189123@163.com).

In this paper, an RSL-TLPMOMA is modeled and analyzed. The laminated coefficient expression of split-laminated is firstly deduced, then the subdomain method is used to analyze RSL-TLPMOMA under no-load conditions. Finally, a prototype is manufactured and tested.

II. Structure of The RSL-TLPMOMA

The cross-sectional view of the RSL-TLPMOMA as shown in Fig.1. It consists of three-phase armature windings with four slots per phase. The PMs are alternatively mounted on the surface of the back iron. The radially split is applied on the stator , the fractional pole-slot and auxiliary-teeth are adopted to reduce the detent force.

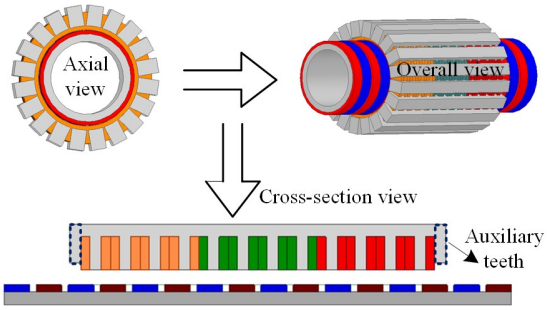

Fig. 1 Radial-split lamination structure of the linear machine

III. Design and Analysis of the RSL-TLPMOMA

A. Discussion the number of split blocks in RSL-TLPMOMA

The stator iron is divided into *n* parts along the circumference. Each part is laminated by several rectangle silicon sheets of steel. The geometric diagram is shown in Fig.2.

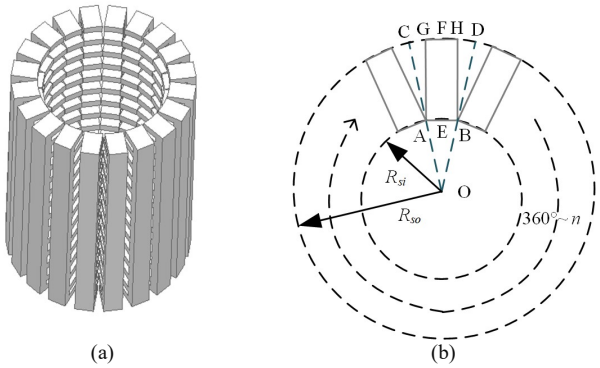

(a) (b)

Fig. 2 Schematic diagram of RSL-TLPMOMA
(a). 3D lamination of RSL
(b). 2D schematic diagram

In Fig. 2 (b), the OCD is each stator unit area after the splitting. The laminated iron cores regions are linear AG, BH, arc GFH and AEB, while ACGA and BDHB regions are voids. To reduce the computer complex, the laminated iron area is approximately equal to the rectangle ABHG area. The area of the ring occupied by each laminated iron is expressed as follows:

$$S_{ABDC} = \pi / n(R_{so}{}^2 - R_{si}{}^2) \tag{1}$$

The actual area of each piece is calculated as follows:

$$S_{ABHG} = 2R_{in}\sin(\pi/n)(R_{so} - R_{si}) \tag{2}$$

So, the lamination coefficient can be expressed as follows:

$$\xi_2 = \xi_1 2n\sin(\pi/n)R_{si} / \pi(R_{so} + R_{si}) \tag{3}$$

And $$\lim_{\substack{n\to\infty \\ R_{s0}\to R_{si}}} \xi_1 2n\sin(\pi/n)R_{si} / \pi(R_{so} + R_{si}) = \xi_1 \tag{4}$$

where, ξ_1 is the traditional laminated coefficient, the empirical values range from 0.9 to 0.98.

The effect of the laminated number and radius ratio on the laminated coefficient is discussed in Fig. 3. It can be found that when the laminated number reaches more than 12, the effect of the laminated factor becomes small, and the radius ratio is the main factor affecting the laminated coefficient. If the internal and external radius of the machine is determined, the number of laminated is preferably at least 12 blocks.

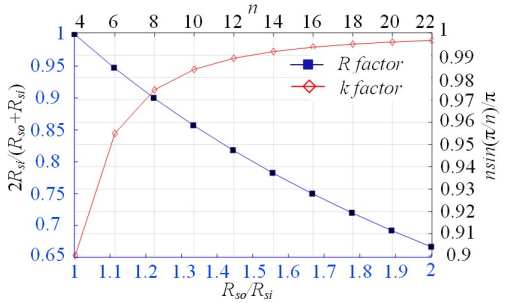

Fig. 3 Laminated coefficient effect by laminated number and radius ratio

B. Subdomain method for magnetic field prediction on no-load condition

In the paper, the subdomain (SD) method is used to estimate the magnetic field of the linear machine. The auxiliary teeth, end effect and entire slot effects are considered. The difference from [11], the slot effect is considered by the SD method which can avoid the crowding effect. A conversion analytical model is established as shown in Fig.4.

Following assumptions are adopted to simply the computation complex as state in [10]. The main parameter is shown in table.1.

TABLE 1
PARAMETERS OF THE RSL-TLPMOMA

Symbol	Parameters	Value
L_s	Axial length of primary	281 mm
L_c	Stator pitch	22 mm
g	Length of air-gap	1 mm
h_m	Thickness of permanent magnet	5mm
L_m	Length of permanent magnet	19 mm
L_f	Width of auxiliary teeth	8.5mm
h_f	Length of auxiliary teeth	28.7 mm
L_p	Pole pitch	24mm

The governing field equation with regard to magnetic potential in different regions is given as follows. And the PM model is calculated based on [29] which is not repeated here.

$$\frac{\partial^2 \mathrm{A}_{1r}}{\partial r^2} + \frac{1}{r}\frac{\partial \mathrm{A}_{1r}}{\partial r} + \frac{1}{r^2}\frac{\partial^2 \mathrm{A}_{1r}}{\partial \theta_s^2} = -\frac{u_0}{r}\left(M_\theta - \frac{\partial M_r}{\partial \theta_s}\right) \quad (i=1) \tag{5}$$

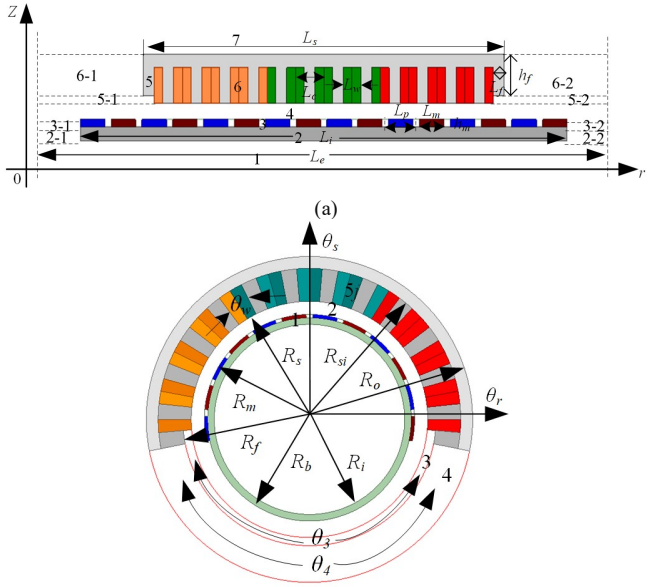

Fig. 4. FEA model and analytical models of the RSL-TLPMOMA
(a). Quasi-2D model in cylindrical coordinates
(b). Subdomain conversion model in polar coordinates

$$\frac{\partial^2 \mathrm{A}_{ir}}{\partial r^2} + \frac{1}{r}\frac{\partial \mathrm{A}_{ir}}{\partial r} + \frac{1}{r^2}\frac{\partial^2 \mathrm{A}_{ir}}{\partial \theta_s^2} = 0 \qquad (i=2...5) \tag{6}$$

By using the separation of variables method, the general solution equations of each subdomain region can be expressed as follows:

In Region 1 (PM region)

$$A_{z1} = A_p(r,\theta_s) + \sum_{k=1}^{\infty}[A_{1k}(r/R_m)^k + B_{1k}(r/R_b)^{-k}]\cos(k\theta_s) + \sum_{k=1}^{\infty}[C_{1k}(r/R_m)^k + D_{1k}(r/R_b)^{-k}]\sin(k\theta_s) \tag{7}$$

where, A_p is a particular solution that can be calculated from [10].

In Region 2 (Air-gap region)

$$A_{z2}=\sum_{k=1}^{\infty}[A_{2k}(r/R_s)^k+B_{2k}(r/R_m)^{-k}]\cos(k\theta_s)+\sum_{k=1}^{\infty}[C_{2k}(r/R_s)^k+D_{2k}(r/R_m)^{-k}]\sin(k\theta_s) \quad (8)$$

In Region 3 (Auxiliary teeth region)

$$A_{z3}=\sum_{u=1}^{\infty}A_{3u}g_{3u}(r)\cos\frac{u\pi}{\theta_3}(\theta_s+\frac{\theta_3}{2}-\pi) \quad (9)$$

where, $g_{3u}(r)=\left(R_s/R_f\right)^{\frac{u\pi}{\theta_3}}(r/R_f)^{\frac{u\pi}{\theta_3}}+(r/R_s)^{-\frac{u\pi}{\theta_3}}$

In Region 4 (End effect regions)

$$A_{z4}=\sum_{m=1}^{\infty}[A_{4m}g_{41m}+B_{4m}g_{42m}]\cos\frac{m\pi}{\theta_4}(\theta_s+\frac{\theta_4}{2}-\pi) \quad (10)$$

where, $g_{41m}=\left(r/R_o\right)^{m\pi/\theta_4}$, $g_{42m}=\left(r/R_s\right)^{-m\pi/\theta_4}$

In Region 5 (slot regions)

$$A_{z5}=\sum_{v=1}^{\infty}A_{5v}g_{5vj}(r)\cos\frac{v\pi}{\theta_w}(\theta_s+\frac{\theta_w}{2}-\pi) \quad (11)$$

where, $g_{5vj}(r)=(R_s/R_{si})^{\frac{v\pi}{\theta_w}}(r/R_{si})^{\frac{v\pi}{\theta_w}}+(r/R_s)^{-\frac{v\pi}{\theta_w}}$. A_{1k}, ~ D_{1k}, A_{2k}~D_{2k}, A_{3u} , A_{4m}, B_{4m} and A_{5v} are integration coefficients that need to be determined. k , m, v represents the difference regions harmonic. θ_3 is the span angle of the auxiliary end region. θ_4 is the span angle of the end region.

The boundary conditions and interface conditions are defined as follows:

$$r=R_b:\ H_{\theta 1}=0 \quad \forall\theta_s \quad (12)$$

$$r=R_m: B_{r1}=B_{r2}, H_{\theta 1}=H_{\theta 2}\ \forall\theta_s \quad (13)$$

$$r=R_s: B_{r2}=B_{r3} \quad \theta_s\in(\pi-\frac{\theta_3}{2},\pi+\frac{\theta_3}{2}) \quad (14)$$

$$r=R_s: H_{\theta 2}\begin{cases}=H_{\theta 3} & \theta_s\in(\pi-\frac{\theta_3}{2},\pi+\frac{\theta_3}{2})\\ 0 & otherwise\end{cases} \quad (15)$$

$$r=R_f: B_{r3}=B_{r4} \quad \theta_s\in(\pi-\frac{\theta_4}{2},\pi+\frac{\theta_4}{2}) \quad (16)$$

$$r=R_f: H_{\theta 3}\begin{cases}=H_{\theta 4} & \theta_s\in(\pi-\frac{\theta_4}{2},\pi+\frac{\theta_4}{2})\\ 0 & otherwise\end{cases} \quad (17)$$

$$r=R_{si}: B_{r2}=B_{r5} \quad \theta_s\in(-\frac{\theta_w}{2}+\theta_j,\frac{\theta_w}{2}+\theta_j) \quad (18)$$

$$r=R_{si}: H_{\theta 3}\begin{cases}=H_{\theta 4} & \theta_s\in(-\frac{\theta_w}{2}+\theta_j,\frac{\theta_w}{2}+\theta_j)\\ 0 & otherwise\end{cases} \quad (19)$$

By applying the boundary conditions and interface conditions above, the unknown integration coefficients can be derived.

IV. Results and Discussion

Due to the circular symmetry principle, only one-twenty of the machine is analyzed, the 3D-FE model is shown in Fig.5. And a prototype machine is fabricated and tested as shown in Fig.6.

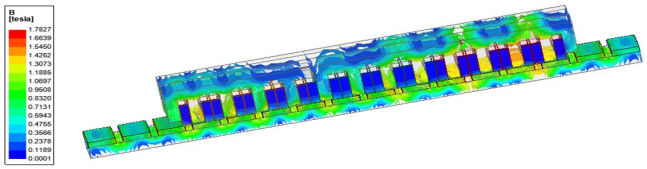

Fig. 5. 3D FE model of RSL-TLPMOMA machine

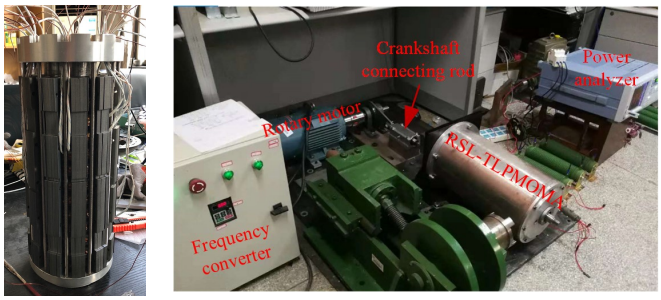

(a) (b)

Fig.6. Prototype and test platform of the RSL-TLPMOMA
(a). RSL structure of the stator
(b). Test platform of test linear machine

Validation of the Analytical Model with FEM And Experiment

According to the previous subdomain conversion method, the flux density distribution of the air gap can be calculated. The radial magnetic flux density distribution of air gap in typical positions is given in Fig.7. From Fig. 7, it can be seen that the analytical method for account of the auxiliary teeth, slot and end effects has good compared with the 3D-FEA method. The small discrepancy between analytical method and FEM solutions might be affected by the radially-split lamination structure of the stator, the effective area of the iron core is reduced in the 3D-FEA model, meanwhile, the nonlinearity of the iron cores is also affecting it.

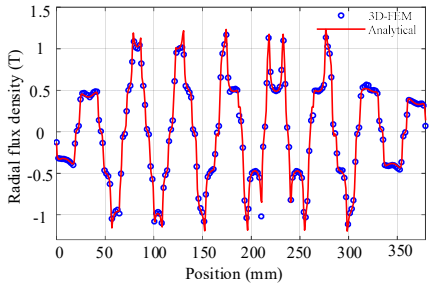

(a)

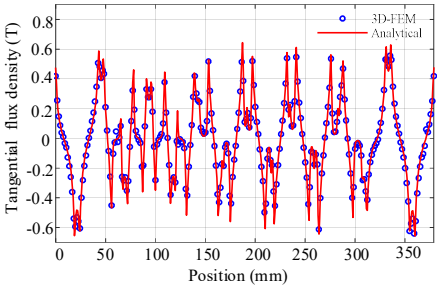

(b)

Fig. 7. Air-gap flux density distribution between the analytical result and the FEA method at the middle position
(a). Radial air-gap flux denstiy distribution
(b). Tangential air-gap flux density distribution

The magnetic flux distribution of the auxiliary-teeth, and end regions when the mover is at the central position are

shown in Fig.8. respectively. It can be inferred from Fig.8 that the radial flux density in the auxiliary teeth region is from 0.2T to 0.8T, and the end regions are from -0.4T to 0.4T, different position has different relative permeances. The tangential flux density of the auxiliary region ranges from -0.4T to 0.45T, and the max value in the end region is about 0.55T. The little deviation is due to the maximum number of harmonic considered and the void effect of stator.

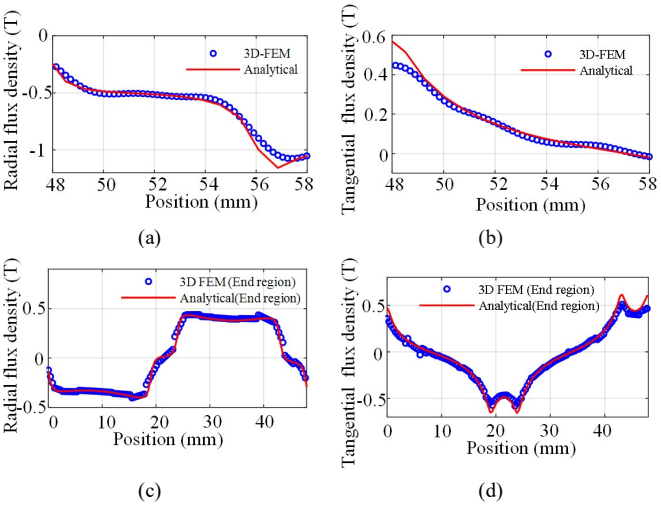

Fig.8. Comparison of the flux density distribution of Aus-region between analytical method and FEA method at the central oscillating position of the machine

(a). Radial flux density of the aux-region
(b). Tangential flux density of the aux-region
(c). Radial flux density of the end-region
(d). Tangential flux density of the end-region

According to the above air-gap flux density, the distributions of the back-EMF obtained from the analytical and 3D-FEA simulation results are compared in Fig. 9. Fig. 9 shows that the amplitude and frequency of the output voltage change continually with time. A comparison of these results indicates that the analytical results are about 4.7% higher than that calculation from the 3D FE model. Since the stator cross-sectional area in the 3D model is reduced compared to those which are implicit in an axis-symmetric model of the same machine.

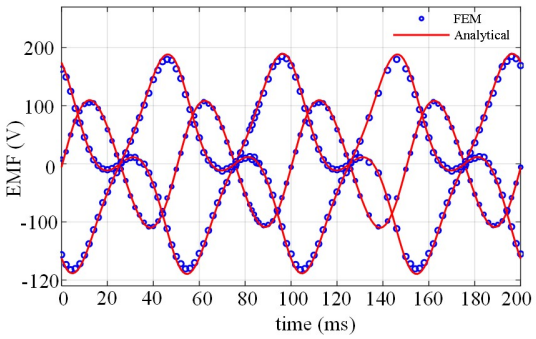

Fig. 9. Distribution of the back-EMF obtained using the analytical and FEM

Fig. 10 shows a comparison of the detent force among the analytical, FEA solutions and experiments. From Fig.10, it can be seen that the detent force from the analytical model and FEM results are in good agreement with the experimental results. The error between theoretical and experimental measurement is 5%. This is because the force is sensitive to the mesh quality in FEM and the analytical model ignored the higher harmonics to reduce the computation time.

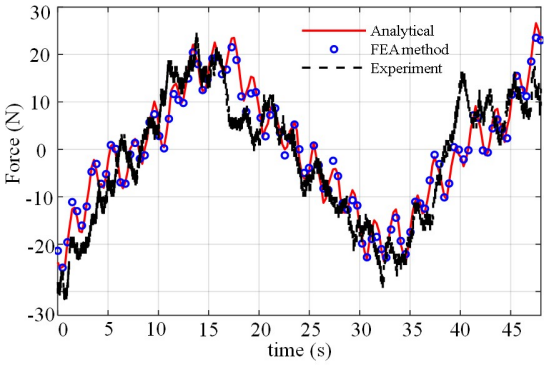

Fig.10. Distribution of the detent force obtained using the analytical, FEM and experiment

V. Conclusion

In the paper, a three-phase tubular linear oscillating generator with a radially-split configuration is modeled and researched. The laminated coefficient expression and the number of the laminated block are deduced. The relationship between the laminated number and radius ratio is discussed. From the discussion, it can be found that the radius ratio is the main factor that affects the laminated coefficient, and when the number of laminated reaches more than 12 blocks, the effect of the laminated factor becomes small. Then, the subdomain conversion method is used to predict the magnetic field under no-load conditions. Good agreement was obtained from the analytical model with the FEM and experiment results. The small discrepancy is mainly from the voids that exist in the stator and the vibration and friction of the experimental platform. The maximum error from the experiment is about 5% which can be accepted. In general, the analytical process offers universal guidance in the initial design of a linear oscillating machine.

ACKNOWLEDGMENT

This work was supported in part by the National Nature Science Foundation of China under 51907027 and in part by the BUCEA Young Scholar Research Capability Improvement Plan under Grant X21081.

Reference

[1] C. A. Oprea, L. Szabó, and C. S. Marţiş, “Linear permanent magnet Electric Generator for Free Piston Engine applications,” in *2012 XXth International Conference on Electrical Machines*, Sep. 2012, pp. 691–696.

[2] J. Chen, Y. Liao, C. Zhang, and Z. Jiang, “Design and ananysis of a permanent magnet linear generator for a free-piston energy converter,” in *2014 9th IEEE Conference on Industrial Electronics and Applications*, Jun. 2014, pp. 1719–1723.

[3] J. Kim, J. Jeong, K. Lee, S. Lee, and J. Choi, “Design and analysis of a linear oscillatory single-phase permanent magnet generator for free-piston stirling engine systems,” in *2016 IEEE Conference on Electromagnetic Field Computation (CEFC)*, Nov. 2016, pp. 1–1.

[4] S. Jeong, W. Oh, H. Lee, S. Cho, and J. Yoo, “The Characteristics of LGE Linear Oscillating Motor,” p. 7, 2010.

[5] K. H. Kim, H. I. Park, S. S. Jeong, S. M. Jang, and J. Y. Choi, “Comparison of Characteristics of Permanent-Magnet Linear

Oscillating Actuator According to Laminated Method of Stator Core," *IEEE Trans. Appl. Supercond.*, vol. 26, no. 4, pp. 1–4, Jun. 2016.

[6] S. W. Seo, G. H. Jang, M. M. Koo, and J. Y. Choi, "Characteristic Analysis of the Influence of Auxiliary Teeth and Notching on the Reduction of the Detent Force of a Permanent Magnet Linear Synchronous Machine," *IEEE Trans. Appl. Supercond.*, vol. 28, no. 3, pp. 1–5, Apr. 2018.

[7] H. Zhang, B. Kou, Z. Q. Zhu, R. Qu, J. Luo, and Y. Shao, "Thrust Ripple Analysis on Toroidal-Winding Linear Permanent Magnet Vernier Machine," *IEEE Trans. Ind. Electron.*, vol. 65, no. 12, pp. 9853–9862, Dec. 2018.

[8] P. Naderi and A. Shiri, "Modeling of Ladder-Secondary-Linear Induction Machine Using Magnetic Equivalent Circuit," *IEEE Trans. Veh. Technol.*, vol. 67, no. 12, pp. 11411–11419, Dec. 2018.

[9] B. Guo, Y. Huang, F. Peng, Y. Guo, and J. Zhu, "Analytical Modeling of Manufacturing Imperfections in Double-Rotor Axial Flux PM Machines: Effects on Back EMF," *IEEE Trans. Magn.*, vol. 53, no. 6, pp. 1–5, Jun. 2017.

[10] H. Hu, J. Zhao, X. Liu, Y. Guo, and J. Zhu, "No-Load Magnetic Field and Cogging Force Calculation in Linear Permanent-Magnet Synchronous Machines With Semiclosed Slots," *IEEE Trans. Ind. Electron.*, vol. 64, no. 7, pp. 5564–5575, Jul. 2017.

[11] R. Guo, H. Yu, and B. Guo, "Analysis of a Tubular Linear Permanent Magnet Oscillator With Auxiliary Teeth Configuration for Energy Conversion System," *IEEE Trans. Transp. Electrification*, vol. 6, no. 2, pp. 602–611, Jun. 2020.